

Efficient Time-Domain Beam-Propagation Method for Modeling Integrated Optical Devices

Husain M. Masoudi, Muhammad A. Al-Sunaidi, and John M. Arnold

Abstract—A new efficient technique that models the behavior of pulsed optical beams in homogenous medium, metallic and dielectric waveguides, is introduced and verified using both linear nondispersive and dispersive examples that have analytical predictions. Excellent accuracy results have been observed. The method is called time-domain beam-propagation method (TD-BPM) because it is similar to the classical continuous-wave BPM with additional time dependence. The explicit finite difference and the Du Fort–Frankel approaches were used to discretize the TD-BPM equation. Comparisons between these techniques are also given with the application of the perfectly matched layers as spatial boundary conditions to the Du Fort–Frankel. Then the TD-BPM was successfully applied to model a two-dimensional dielectric Y-junction. It is concluded that the new technique is more efficient than the traditional finite-difference TD method, especially in modeling large optical devices.

Index Terms—Beam-propagation method (BPM), finite-difference analysis, modeling, numerical analysis, optical waveguide theory, partial differential equation, pulse propagation, time domain (TD).

I. INTRODUCTION

THE INTEGRATION of a large number of optical devices, for processing optical communication signals, makes the ability to analyze, understand, and predict the behavior of such circuits a difficult task that needs to be resolved. There are a number of reasons for this difficulty. First, many of the optical devices are designed on the basis of nonlinear optical interaction of $\chi^{(2)}$ or $\chi^{(3)}$ responses of the material, which require careful understanding due to the complexity of these phenomena. The second reason is that most of the applications require pulsed optical beams rather than continuous-wave (CW) operation, where less progress is made to analyze time-domain (TD) problems. It is worth mention that in most cases, analyzing TD interactions is more difficult than CW problems because of the large spectrum of frequencies involved in the TD. The third, and probably the most important, reason is that most of these devices are of a three-dimensional (3-D) nature with length of interaction taking place over 10^4 optical wavelength or longer. For these reasons, efficient algorithms are required to analyze such devices accurately. Pulse propagation in optical structures can

be analyzed, in principle, using the finite-difference time-domain (FDTD) method [1]–[5]. The technique was used to model two-dimensional optical waveguides and showed to be suitable to some electromagnetic problems in particular microwave and optical devices [1]–[8]. While this method combines features of scattering problems, it requires enormous computer resources (execution time and memory) even for simple two-dimensional structures [5]–[8]. For a typical 3-D optical waveguide of spatial sizes around $10 \mu\text{m}$ by $10 \mu\text{m}$ and 3 mm interaction length, the FDTD requires $\lambda/30$ spatial step size that keeps numerical dispersion at its minimum, where λ is the guide wavelength [34]. This results in $300 \times 300 \times 90\,000 = 8.1 \times 10^9$ numerical cells for an optical wavelength of $\lambda = 1 \mu\text{m}$. The FDTD consumes 24 memory words per cell, which makes the total memory 1.944×10^{11} words. It is to be noted that these figures increase with the decrease of λ . In addition, the total efficiency is dependant on the time iterations. It is known that the Courant-Friedrichs and Lewy (CFL) stability requirements [1]–[5], [34] restrict the time step size to

$$\Delta t \leq \frac{1}{c_{\max}} \left[\frac{1}{\Delta x^2} + \frac{1}{\Delta y^2} + \frac{1}{\Delta z^2} \right]^{-1/2}$$

which is equal to 0.06 fs for the parameters given above. Considering a Gaussian time pulse of 100-fs half-pulse width and a time window of 600 fs for only the total pulse to be fully excited inside the problem space, which gives 10 000 time steps. Obviously, this would overwhelm existing high-performance computer machines (supercomputers) [20]–[24]. To overcome these difficulties, considerable work has been done to model devices using only one unknown field (based on the wave equation) rather than six unknown fields (based on Maxwell's equations) as in the FDTD [9]–[14]. This will result in a large saving in terms of computer execution time and storage space, especially for three-dimensional analysis. Recently, slow wave simulators have been proposed that depend on slowly time-varying envelope variation [9]–[13]. These techniques are not suitable for modeling pulse propagation, which requires the fast variation of the pulse envelope to be accounted for. A more interesting approach [14] uses Fourier analysis to advance the pulse using the beam-propagation method (BPM) style [15]–[17]. The technique writes the wave equation in the spectral domain, wherein each frequency of the pulsed beam is propagated to the desired distance and the new pulse shape is reconstructed using the inverse fast Fourier transform (FFT). However, this approach is restricted to linear optical interaction problems. In this paper, we show that using the classical explicit finite-difference (EFD) BPM approach [18], [19] to

Manuscript received January 4, 2000; revised September 26, 2000. This work was supported by King Fahd University of Petroleum and Minerals, Dhahran, Saudi Arabia.

H. M. Masoudi and M. A. Al-Sunaidi are with the Optical Device Simulation Group, Department of Electrical Engineering, King Fahd University of Petroleum and Minerals (KFUPM), Dhahran, Saudi Arabia (e-mail: husainm@kfupm.edu.sa; msunaidi@kfupm.edu.sa).

J. M. Arnold is with the Department of Electronics and Electrical Engineering, University of Glasgow, Glasgow, Scotland, U.K.

Publisher Item Identifier S 0733-8724(01)03630-1.

solve the time-domain wave equation will lead to a simple and efficient technique to accurately analyze pulse propagation in optical waveguides. The CW EFD-BPM is known for its simplicity, high efficiency, accuracy, and suitability for parallel implementations especially for modeling three-dimensional optical devices [18]–[21]. In addition, the technique proved to be very reliable in modeling three-dimensional devices containing second-order nonlinear optical interaction of $\chi^{(2)}$ [22]–[24].

The proposed time-domain BPM (TD-BPM) involves writing the time-domain wave equation as a one-way paraxial equation for the propagation along the axial direction z . This arrangement has the advantage of allowing the numerical time window to follow the evolution of the pulse and hence minimizes the computer storage of the problem as well as the execution time. The real-valued scalar wavefunction ψ is factored into a product of the carrier frequency oscillation and a complex modulating envelope Ψ in the form

$$\psi(\mathbf{x}, t) = \Psi(\mathbf{x}, t)e^{ikz}e^{-i\omega t} + \Psi^*(\mathbf{x}, t)e^{-ikz}e^{i\omega t}$$

and getting the wave equation for the complex envelope Ψ . Applying paraxial approximation to the wave equation, by neglecting derivatives with respect to the axial dimension z higher than the first derivatives while keeping all time variation intact, leads to a one-way propagation of a BPM style equation. This makes the time dependence of the complex envelope, as it is another transverse variable in addition to the two spatial dimensions. It is to be noticed that the propagation is essentially in one direction, $z = +\infty$, but the complex envelope is not necessarily assumed to be slowly varying in time t . We have used the EFD to discretize the time-domain BPM equation (an early result of this technique [EFD-TD] was reported in a communication letter [25]). On the other hand, we have also found that modifying the EFD-TD equation, using the Du Fort–Frankel approach [26], improves the efficiency of the technique while retaining the same accuracy and features [24], [27], [28]. Throughout the following, for simplicity we will refer to the Du Fort–Frankel technique as modified EFD-TD (or MEFD-TD). The advantages of the MEFD-TD over the EFD-TD are:

- 1) the longitudinal step Δz can be relaxed more;
- 2) the total mesh points can be divided into two equal sets, where only one set can be used for computation (50% saving) and the same accuracy is retained;
- 3) perfectly matched layers (PMLs) can be used as an absorbing spatial boundary condition.

Some of these advantages have been observed with the CW MEFD [24], [27], [28]. The purpose of this paper is to characterize the TD-BPM as a new technique for modeling pulsed optical beams using both the EFD-TD and the MEFD-TD and to look at the prospect of analyzing long 3-D optical devices.

In the next section, the time-domain method (TD-BPM) equations will be derived from the wave equation. Section III shows the details of discretizing the TD-BPM method using the EFD-TD and the MEFD-TD, with main differences pointed out. Section IV shows rigorous examinations for the numerical techniques using three different and practical problems. First, the method is applied to simple propagation of a pulsed

Gaussian beam in homogenous medium (nondispersive), and the results are compared with analytical results. Then the method is applied to dispersive linear guided-wave problems, where the correct behavior of the wave can be predicted analytically, and again the results are compared with the theoretical predictions. Propagation of pulsed guided beams in metallic waveguides and dielectric waveguides is considered. Later in the section, the introduction of the PML technique, as spatial boundary conditions, to the MEFD-BPM is shown with a simple dielectric waveguide example. In Section V, the simulation of pulsed optical beams in a dielectric Y -junction waveguide is shown.

II. THEORY

We start with the scalar time-domain wave equation

$$\nabla^2\psi - \frac{n^2}{c_o^2}\partial_t^2\psi = 0 \quad (1)$$

where

- $n = n(\mathbf{x})$ position-dependent refractive index variation;
- ∇^2 spatial Laplacian operator;
- c_o wave velocity in free space.

It is assumed that the vector nature of the field can be ignored, which is a good first approximation for the paraxial problems of the type considered here that is appropriate for the BPM [15]–[17]. A carrier frequency ω and a propagation coefficient $k = k_o n_o$ in the direction of propagation are extracted from ψ as

$$\psi = \Psi e^{ikz} e^{-i\omega t} + \text{c.c.} \quad (2)$$

where

- $k_o = \omega/c_o$;
- n_o reference refractive index;
- c.c. complex conjugate of the expression preceding it.

Introducing the standard parabolic approximation by neglecting second derivatives of the wavefunction with respect to the axial coordinate z , the scalar wave equation (1) becomes

$$2i \left(k\partial_z\Psi + \frac{n^2}{c_o^2}k_o\partial_t\Psi \right) + (n^2k_o^2 - k^2)\Psi - \frac{n^2}{c_o^2}\partial_t^2\Psi + \nabla_{\perp}^2\Psi = 0. \quad (3)$$

As mentioned before, one of the interesting features of the TD-BPM is the application of the moving time window technique. A compact pulse eventually disappears from the window after a certain number of propagation steps, where it requires the computational window to be adjusted in time at each propagation step so as to effectively move at the group velocity of the pulse envelope. The substitution of a moving time coordinate $\tau = t - v_g^{-1}z$ with arbitrary v_g changes (3) to

$$2i \left\{ k\partial_z\Psi + k_o \left(\frac{1}{c} - \frac{1}{v_g} \right) \partial_{\tau}\Psi \right\} + (n^2k_o^2 - k^2)\Psi - \frac{n^2}{c_o^2}\partial_{\tau}^2\Psi + \nabla_{\perp}^2\Psi = 0. \quad (4)$$

III. NUMERICAL TECHNIQUES

A. The Explicit FD Time-Domain BPM

Using the central finite-difference approximations

$$\begin{aligned}
\partial_z \Psi(x, y, z, \tau) &\rightarrow \frac{1}{2\Delta z} (\Psi(x, y, z + \Delta z, \tau) \\
&\quad - \Psi(x, y, z - \Delta z, \tau)) \\
\partial_\tau \Psi(x, y, z, \tau) &\rightarrow \frac{1}{2\Delta \tau} (\Psi(x, y, z, \tau + \Delta \tau) \\
&\quad - \Psi(x, y, z, \tau - \Delta \tau)) \\
\partial_\tau^2 \Psi(x, y, z, \tau) &\rightarrow \frac{1}{\Delta \tau^2} (\Psi(x, y, z, \tau + \Delta \tau) \\
&\quad + \Psi(x, y, z, \tau - \Delta \tau) \\
&\quad - 2\Psi(x, y, z, \tau)) \\
\nabla_\perp^2 \Psi(x, y, z, \tau) &\rightarrow \frac{1}{\Delta x^2} (\Psi(x + \Delta x, y, z, \tau) \\
&\quad + \Psi(x - \Delta x, y, z, \tau)) \\
&\quad + \frac{1}{\Delta y^2} (\Psi(x, y + \Delta y, z, \tau) \\
&\quad + \Psi(x, y - \Delta y, z, \tau)) \\
&\quad - 2 \left(\frac{1}{\Delta x^2} + \frac{1}{\Delta y^2} \right) \Psi(x, y, z, \tau) \quad (5)
\end{aligned}$$

to replace the partial derivatives in (4) leads to the second-order accurate EFD-TD

$$\begin{aligned}
\Psi_{p,j,m}(z + \Delta z) &= \Psi_{p,j,m}(z - \Delta z) \\
&\quad + a_x [\Psi_{p-1,j,m}(z) + \Psi_{p+1,j,m}(z)] \\
&\quad + a_y [\Psi_{p,j-1,m}(z) + \Psi_{p,j+1,m}(z)] \\
&\quad + a_\tau [\Psi_{p,j,m-1}(z) + \Psi_{p,j,m+1}(z)] \\
&\quad + a_{\tau\tau} [\Psi_{p,j,m-1}(z) - \Psi_{p,j,m+1}(z)] \\
&\quad + b_{p,j} \Psi_{p,j,m}(z) \quad (6)
\end{aligned}$$

where

$$\begin{aligned}
a_z &= -\frac{\Delta z}{ik_o n_o}, \quad a_x = \frac{a_z}{\Delta x^2}, \quad a_y = \frac{a_z}{\Delta y^2}, \\
a_\tau &= \frac{-n_{p,j}^2 a_z}{c^2 \Delta \tau^2}, \quad a_{\tau\tau} = \frac{i\omega n_{p,j}^2 a_z}{c^2 \Delta \tau}, \\
b_{p,j} &= a_z \left[-\frac{2}{\Delta x^2} - \frac{2}{\Delta y^2} + \frac{2n_{p,j}^2}{c^2 \Delta \tau^2} + k_o^2 (n_{p,j}^2 - n_o^2) \right].
\end{aligned}$$

p , j , and m represent the discretization of x , y , and τ , respectively. The discretized equation (6) is very similar to the classical CW equation [18]–[21], but with an additional transverse variable τ ; if the field ψ is time independent, then the EFD-TD reverts to the CW case. The explicit propagation of the optical field using the EFD-TD is straightforward since it involves a multiplication of the input field with a very sparse matrix with only five elements in each row, which makes the method very efficient and highly parallel [20], [21]. As in [19], the stability

analysis of the algorithm can be found by searching for discretized plane wave solutions of (6) under the condition of a uniform medium and determining conditions under which these plane waves can have real propagation coefficients. The characteristic equation for the propagation coefficient β of such a discretized plane wave

$$\begin{aligned}
\Psi &= \exp(i\beta s \Delta z) \exp(i\gamma_x m_x \Delta x) \\
&\quad \cdot \exp(i\gamma_y m_y \Delta y) \exp(-i\Omega m_\tau \Delta \tau) \quad (7)
\end{aligned}$$

assuming that n is independent of position \mathbf{x} , $nk_o = k$, and $v_g = c$, is

$$\begin{aligned}
-2 \left(k \frac{\sin \beta \Delta z}{\Delta z} \right) - \frac{4 \sin^2 \frac{1}{2} \Omega \Delta \tau}{c^2 \Delta \tau^2} + \frac{4 \sin^2 \frac{1}{2} \gamma_x \Delta x}{\Delta x^2} \\
+ \frac{4 \sin^2 \frac{1}{2} \gamma_y \Delta y}{\Delta y^2} = 0. \quad (8)
\end{aligned}$$

It is required that this equation have solutions for which $-1 < \sin \beta \Delta z < 1$ to permit real values of β ; this shows that the algorithm is stable under the condition

$$\begin{aligned}
-\frac{k}{\Delta z} < -\frac{2 \sin^2 \frac{1}{2} \Omega \Delta \tau}{c^2 \Delta \tau^2} + \frac{2 \sin^2 \frac{1}{2} \gamma_x \Delta x}{\Delta x^2} + \frac{2 \sin^2 \frac{1}{2} \gamma_y \Delta y}{\Delta y^2} \\
< \frac{k}{\Delta z}. \quad (9)
\end{aligned}$$

This is satisfied for all Ω , γ_x and γ_y if

$$\frac{2}{\Delta x^2} + \frac{2}{\Delta y^2} < \frac{k}{\Delta z}, \quad \frac{2}{c^2 \Delta \tau^2} < \frac{k}{\Delta z}. \quad (10)$$

B. The Modified Explicit FD Time-Domain BPM

From the CW numerical experience, accurate modeling of practical optical devices requires that Δx and Δy be much smaller than the optical carrier wavelength, resulting in a very small propagation step size Δz according to the above condition in (10) [16]–[21]. However, if the field $\Psi_{p,j,m}(z)$ in (6) is replaced by its average value [26]–[28]

$$\Psi_{p,j,m}(z) = [\Psi_{p,j,m}(z + \Delta z) + \Psi_{p,j,m}(z - \Delta z)]/2 \quad (11)$$

this gives the following Du Fort–Frankel technique

$$\begin{aligned}
\Psi_{p,j,m}(z + \Delta z) &= c_{p,j} \Psi_{p,j,m}(z - \Delta z) \\
&\quad + d_{p,j}^x [\Psi_{p-1,j,m}(z) + \Psi_{p+1,j,m}(z)] \\
&\quad + d_{p,j}^y [\Psi_{p,j,m-1}(z) + \Psi_{p,j,m+1}(z)] \\
&\quad + f_\tau [\Psi_{p,j,m-1}(z) + \Psi_{p,j,m+1}(z)] \\
&\quad + f_{\tau\tau} [\Psi_{p,j,m-1}(z) - \Psi_{p,j,m+1}(z)] \quad (12)
\end{aligned}$$

where

$$\begin{aligned}
c_{p,j} &= (2 + b_{p,j}) / (2 - b_{p,j}) \\
d_{p,j}^x &= 2a_x / (2 - b_{p,j}), \quad d_{p,j}^y = 2a_y / (2 - b_{p,j}) \\
f_\tau &= 2a_\tau / (2 - b_{p,j}), \quad f_{\tau\tau} = 2a_{\tau\tau} / (2 - b_{p,j}).
\end{aligned}$$

The Du Fort–Frankel (MEFD-TD) method is unconditionally stable in a uniform medium with $n^2 = n_o^2$, in contrast to the conditional stability of the standard explicit discretization in (10) [28]. We may notice from the EFD-TD and the MEFD-TD equations [(6) and (12)] that the two methods require two initial fields to start the propagation. It is known that the CW MEFD produces, for large longitudinal step size Δz , little spurious fields if the two initial fields are equal or excited with other BPMs [28]. Two numerical solutions have been suggested to reduce or eliminate the spurious field. If the initial field is a guided mode, two initial fields $\Psi(0)$ and $\Psi(\Delta z)$ spaced by Δz can be found by multiplying $\Psi(0)$ with the appropriate phase factor to obtain $\Psi(\Delta z)$, assuming that the medium in the longitudinal direction does not change. The other technique is to use two equal initial fields with a very small initial step size Δz increasing gradually to the desired Δz . As the initial Δz decreases, the error of the spurious field reduces [28]. The same behavior was observed with the MEFD-TD.

There are three major advantages for the MEFD-TD over the EFD-TD. The first is that the longitudinal step Δz can be much more relaxed than the condition in (10) where more than ten times larger step size can be achieved with very little accuracy degradation [28]. The second advantage is in using the leapfrog arrangement [24], [27], [28], where the total mesh points of the MEFD-TD can be divided into two equal sets (even and odd) in which only one set could be used in the computation while retaining the same accuracy. This gives the MEFD-TD a further 50% increase in the speed per propagational step over the EFD-TD. Experiments with both methods showed that the EFD-TD becomes unstable if PML layers are introduced as an absorbing boundary condition in the spatial dimension. On the other hand, the PML can be used with the MEFD-TD algorithm, as will be shown in the next section. In this work, the PML has been used by representing the transverse spatial dimension with a lossy coordinate as [29], [30]

$$\hat{x} = x \left(1 + i \frac{\sigma_x}{\omega \epsilon_o n_p} \right) \quad (13)$$

where n_p is the refractive index of the PML medium, which can be chosen to be equal to that of the medium next to the PML layer and σ_x is the conductivity of the PML layer.

IV. NUMERICAL ANALYSIS

In this section, we rigorously test the numerical techniques discussed in Section III using three different practical problems. The first is the propagation of a pulsed beam in free space; the second is the propagation of pulsed guided modes in metallic waveguides; and the third is the propagation of pulsed guided modes in dielectric waveguides. Throughout the following simulations, a temporal pulse of the form

$$F(\tau) = \exp \left\{ - \left(\frac{\tau}{\sigma_{to}} \right)^2 \right\} \quad (14)$$

is considered and the initial field at $z = 0$ is assumed to be equal to

$$\Psi(x, y, z = 0, \tau) = \Psi_o(x, y)F(\tau) \quad (15)$$

where σ_{to} scales the duration of the initial pulse in the time domain and $\Psi_o(x, y)$ is the transverse spatial profile of the pulsed beam at $z = 0$. In addition to the transverse spatial boundary conditions, time-domain boundary conditions for the fields are also required. It is also necessary to compensate for the displacement of the pulse in the time window as z advances, due to the motion of the envelope Ψ at the group velocity. For simplicity, unless otherwise stated, the spatial boundary conditions $\Psi(\pm M_x \Delta x, \pm M_y \Delta y, s \Delta z, m_\tau \Delta \tau) = 0$ on a rectangular boundary surrounding the structure have been chosen. This is used in simulations that involve no scattering effects, and the field is expected to be zero at the spatial boundary. We have investigated two simple methods of applying temporal boundary conditions. The first involves what is called a moving window technique. Zero boundary conditions $\Psi = 0$ at $\tau = \pm M_\tau \Delta \tau$ are applied in the relative time window (coordinate τ) while moving in the absolute time frame (coordinate t) with the velocity of the pulse, so that the relative motion of the pulse in the time window is eliminated. On the other hand, the required group velocity v_g is not known in advance of the computation for a number of optical propagation problems, and has to be generated dynamically as the propagation progresses. Incorrect movement to the time window results in the disappearance of the pulse from the numerical window after a certain number of propagation steps. Another interesting technique is the application of periodic boundary conditions at the ends of the relative time window, so that a pulse leaving the window at one side simply reenters at the other side even if the correct velocity is not known precisely. Both of these techniques were tested and proved quite workable and efficient; they both permit the time window to be of a finite extent $2M_\tau \Delta \tau$ on the order of a few pulse widths.

Experimental results for the two techniques (the EFD-TD and the MEFD) showed that they both converge to a similar result when both use the same longitudinal Δz , where Δz for the EFD-TD is below the stability condition of the algorithm. The same behavior was confirmed in the CW cases [28]. To concentrate on the temporal aspect of characterizing the methods, the MEFD-TD will always be excited with a small and uniform Δz that ensures the reduction/elimination of any spurious field mentioned before. Comparison between the results of the two techniques will be shown later in the section (see Fig. 4).

A. Homogenous and Nondispersive Medium

In the first example, a pulsed Gaussian beam is propagated in a two-dimensional (x and z) free-space medium using the TD-BPM, and the numerical results are compared with analytical results. With an initial spatial Gaussian waist w_o at $z = 0$, the evolution of each frequency component of the spectrum of the wavefunction in free space is given in the frequency domain as [31]

$$\begin{aligned} \tilde{\Psi}(x, z, \omega) = & \Psi_o \frac{w_o}{w(z)} \\ & \cdot \exp \left\{ i [kz - \eta(z)] - x^2 \left[\frac{1}{w^2(z)} - \frac{ik}{2R(z)} \right] \right\} \end{aligned} \quad (16)$$

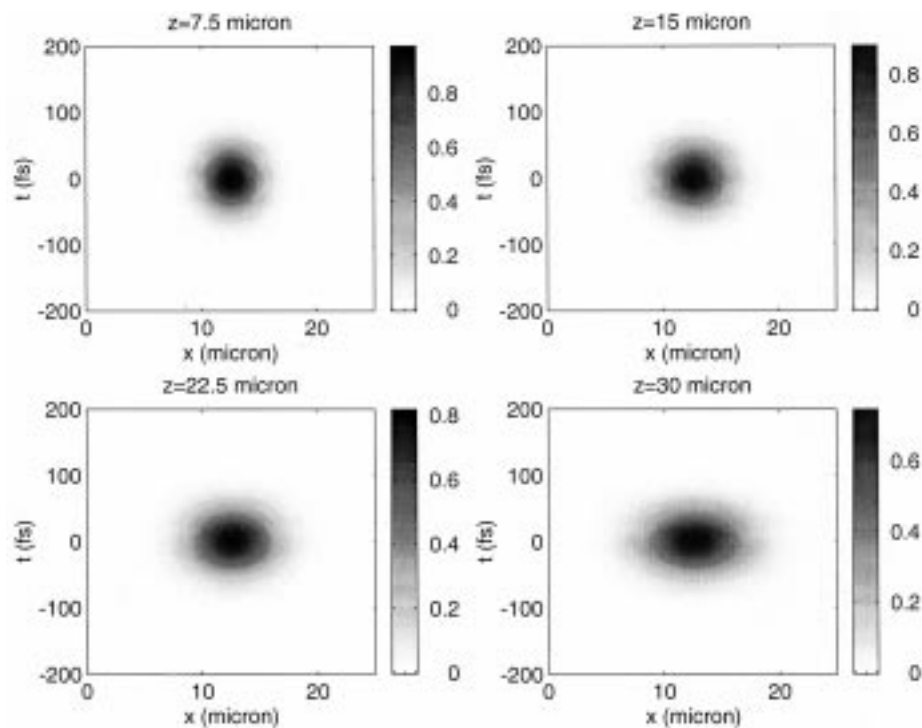


Fig. 1. The evolution of the pulsed Gaussian beam in free space using the EFD-TD. The initial Gaussian waist was $w_o = 2.5 \mu\text{m}$, an initial pulse width of $\sigma_{t_o} = 50 \text{ fs}$, and $\lambda = 1.0 \mu\text{m}$. The reference refractive index was chosen to be $n_o = 1.0$, $\Delta x = 0.1 \mu\text{m}$, $\Delta\tau = 1.0 \text{ fs}$, and $\Delta z = 0.025 \mu\text{m}$. A moving time window was used to follow the pulse.

for $z \ll z_o$, where the waist, the radius of curvature, the phase term, and the diffraction length, respectively, are given by

$$w^2(z) = w_o^2 \left[1 + \left(\frac{\lambda z}{\pi w_o^2} \right)^2 \right] = w_o^2 \left(1 + \frac{z^2}{z_o^2} \right)$$

$$R(z) = z \left[1 + \left(\frac{\pi w_o^2}{\lambda z} \right)^2 \right] = z \left(1 + \frac{z_o^2}{z^2} \right)$$

$$\eta(z) = \tan^{-1} \left(\frac{\lambda z}{\pi w_o^2} \right) = \tan^{-1} \left(\frac{z}{z_o} \right)$$

$$z_o = \frac{\pi w_o^2}{\lambda} = \left(\frac{w_o^2}{2c} \right) \omega.$$

The evolution of a pulsed Gaussian beam in free space can be found from (16) by the inverse Fourier transform of the product of $\tilde{\Psi}$ and the Fourier transform of (14), which can be written as

$$\Psi(x, z, t) = \frac{1}{2\pi} \int_{-\infty}^{\infty} \tilde{\Psi}(x, z, \omega) \tilde{F}(\omega) e^{-i\omega t} d\omega \quad (17)$$

where $\tilde{F}(\omega)$ is the Fourier transform of (14) (see [31] for details). This technique was used to validate the results of the TD-BPM where a computer program, using FFT, was developed to find the electric field at any propagation distance z . Fig. 1 shows plots for the field of a pulsed Gaussian beam that has been propagated to a distance of $z = 30 \mu\text{m}$ using the EFD-TD. The initial spatial Gaussian waist was $w_o = 2.5 \mu\text{m}$, the initial pulse width $\sigma_{t_o} = 50 \text{ fs}$, and the wavelength of the carrier frequency $\lambda = 1.0 \mu\text{m}$. The reference refractive index was chosen to be $n_o = 1.0$. In general, we have observed that the results of Fig. 1 are very similar to the results of the MEFD-TD and

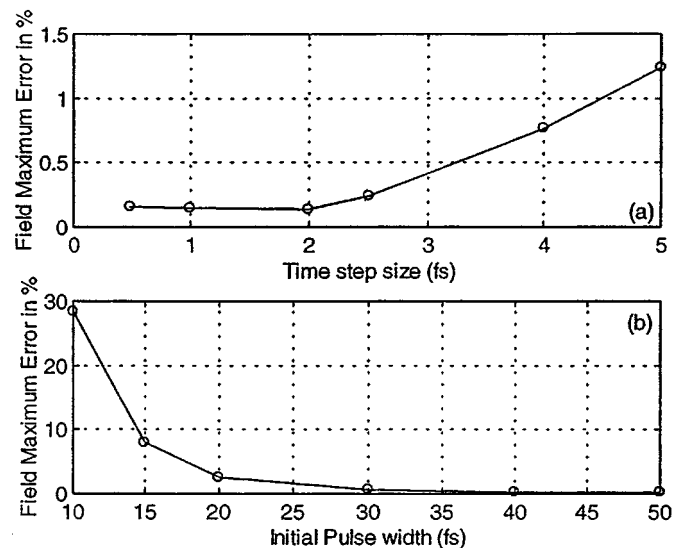


Fig. 2. The percentage maximum error in the field at a distance of $z = 30 \mu\text{m}$ as a function of (a) the time step size $\Delta\tau$ and (b) the initial pulse width σ_{t_o} . Other parameters are the same as those of Fig. 1.

of (17). The figure shows that the waist spreads to a value of $w(30 \mu\text{m}) = 4.565 \mu\text{m}$, which agrees with the analytical results. On the other hand, the pulse width in the time domain is unchanged, which is predicted by the analytical results because the medium is nondispersive. A moving window in the time domain was used to follow the propagation of the pulse in free space. The window was moved with the group velocity, which is equal to the phase velocity of light in free space for this particular example. Other tests were made on the numerical parameters of the method (i.e., Δx , $\Delta\tau$, and Δz). The free-space

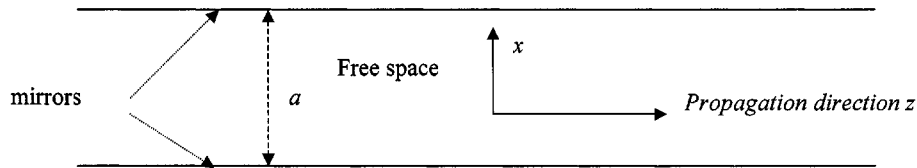


Fig. 3. The two-dimensional metallic waveguide used in the analysis.

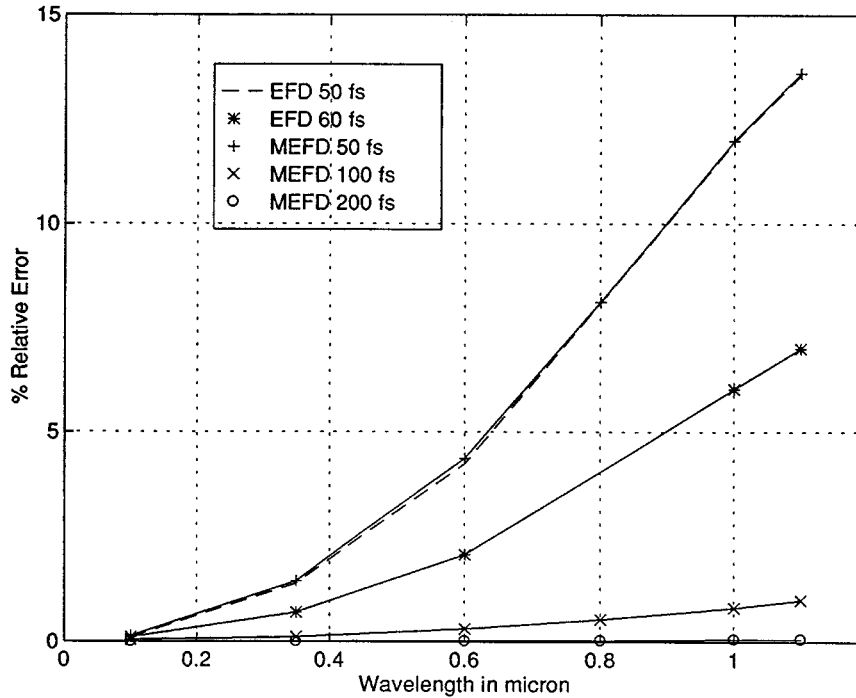


Fig. 4. The percentage relative error of the pulse width versus the carrier wavelength for different initial pulse widths using the EFD-TD and the MEFD-TD. The calculations were performed at $z = 332 \mu\text{m}$ with $\epsilon_r = 1.0$ and $\mu_r = 1.0$.

case showed that the method is not sensitive to the change in Δx and Δz , provided that Δz is below the limit of stability in (10) (with $\Delta y \rightarrow \infty$). Fig. 2(a) shows the percentage maximum error in the field as a function of $\Delta\tau$. From the figure, it is clear that the technique converges as $\Delta\tau$ decreases. Fig. 2(b) shows the effect in reducing the initial pulse width. It is clear from the figure that the method cannot cope with ultrashort pulses, and this limitation will be understood from the following examples.

B. Metallic Waveguide

To test the TD-BPM in waveguide problems, a two-dimensional (x and z) metallic waveguide, shown in Fig. 3, was used for that purpose. The metallic waveguide was chosen because of the availability of theoretical predictions. It is known that the cutoff frequency of this waveguide depends on the width of the waveguide as [32]

$$\omega_c = \frac{q\pi v}{a}, \quad q = 1, 2, 3, \dots \quad (18)$$

where $v = (\epsilon \mu)^{-1/2}$ and the cutoff wavelength $\lambda_c = 2a/q$ measured at the velocity of light in the material between the two metallic waveguides. The material of the waveguide, between

the two mirrors, was taken to be free space. The phase velocity of the guided mode is given as

$$v_p = \frac{\omega}{\beta} = \frac{v}{\sqrt{1 - (\omega_c/\omega)^2}} \quad (19)$$

with a propagation constant

$$\beta = \frac{\omega}{v} \sqrt{1 - (\omega_c/\omega)^2} \quad (20)$$

and the exact group velocity of the signal can be calculated as

$$v_g = \frac{d\omega}{d\beta} = v \sqrt{1 - (\omega_c/\omega)^2}. \quad (21)$$

Consider a pulsed first guided mode ($q = 1$) to propagate inside the structure of Fig. 3. The temporal pulse width at a distance z can be measured as [32]

$$\sigma_t(z) = \sigma_{t0} \sqrt{1 + \left(\frac{2z}{\sigma_{t0}^2} \frac{d^2\beta}{d\omega^2} \right)^2} \quad (22)$$

where the dispersion term can be calculated from (21) using the following relation:

$$\frac{d^2\beta}{d\omega^2} = \frac{-(\omega_c^2/\omega^3)}{v[1 - (\omega_c/\omega)^2]^{3/2}}. \quad (23)$$

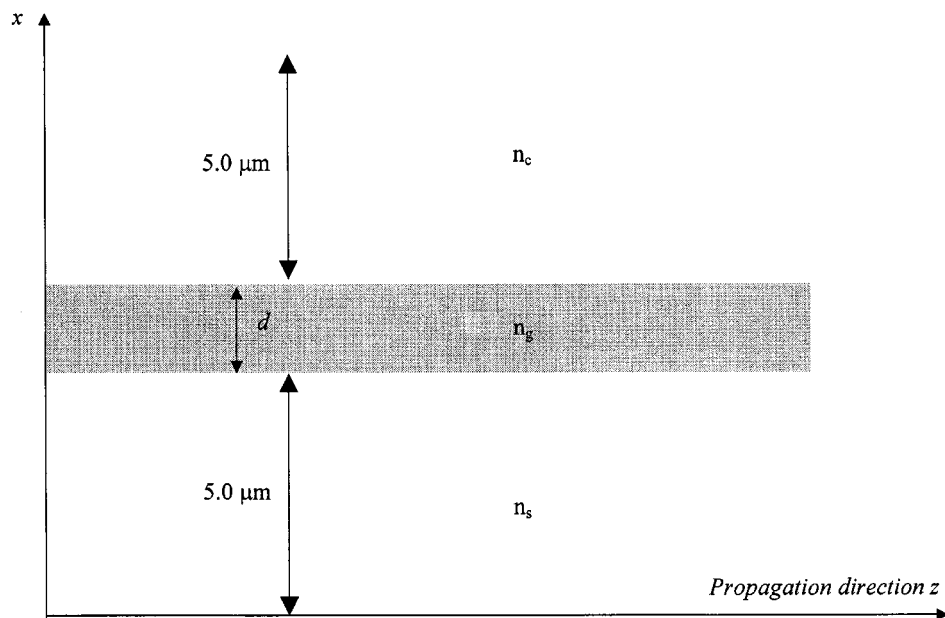


Fig. 5. The two-dimensional slab dielectric waveguide used in the analysis. $n_g = 1.2$, $n_s = n_c = 1.0$, and $\lambda = 1.0 \mu\text{m}$.

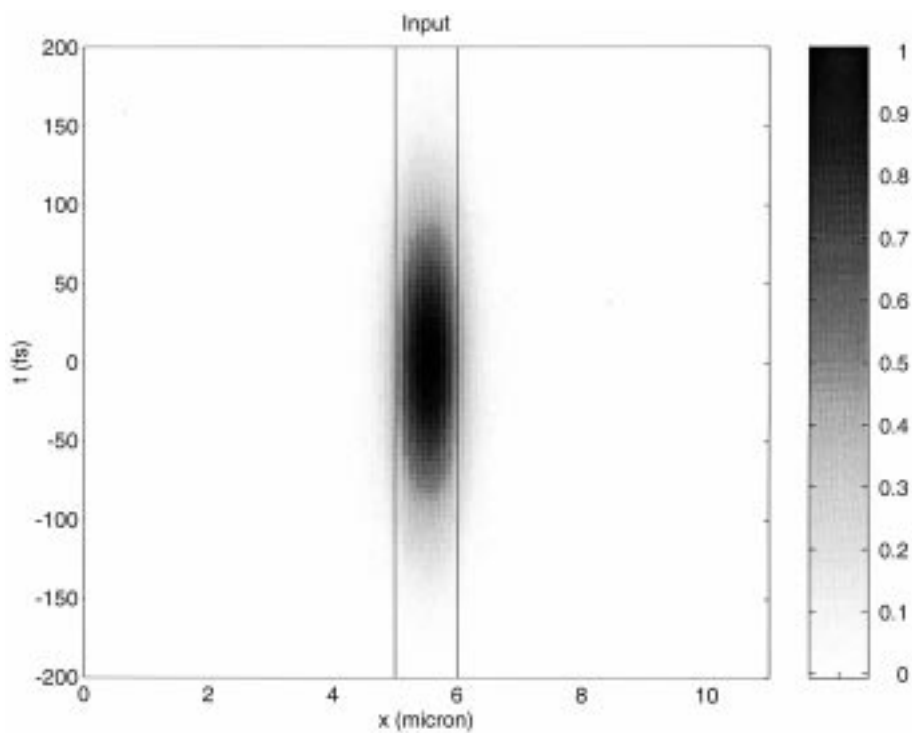


Fig. 6. The input field used in the analysis. The field consists of a pulsed first guided mode with an initial pulse width of $\sigma_{t_0} = 100$ fs. The total time window used was 600 fs (for clarity only 400 fs is shown), and the two vertical lines show the position of the slab waveguide with $d = 1 \mu\text{m}$.

For a waveguide width of $a = 1.0 \mu\text{m}$, the cutoff wavelength $\lambda_c = 2 \mu\text{m}$ and the first guided mode in the transverse direction x can be written as $\Psi_o(x) = \sin(\pi x/a)$. Numerical observations of the TD-BPM showed that the reference propagation coefficient k should be chosen to be equal to the propagation coefficient β of the guided mode in order that the pulse travels with the correct velocity and hence be stationary in the relative time window. The group velocity was measured numerically by calculating the velocity of the pulse peak and then compared with (21). Fig. 4 shows the relative

error in percent versus the carrier wavelength at $z = 332 \mu\text{m}$ for different initial pulse widths using the MEFD-TD and EFD-TD. The results of the EFD-TD are those appearing in [25]. As mentioned earlier, the figure shows that the results of the EFD-TD and MEFD-TD are very similar. It is to be mentioned that increasing the carrier wavelength will increase the propagation angle $\theta = \arcsin(\lambda/\lambda_c)$, with respect to the axial direction, of the guided plane waves forming the mode inside the waveguide, making the mode less paraxial. On the other hand, increasing the wavelength decreases the number

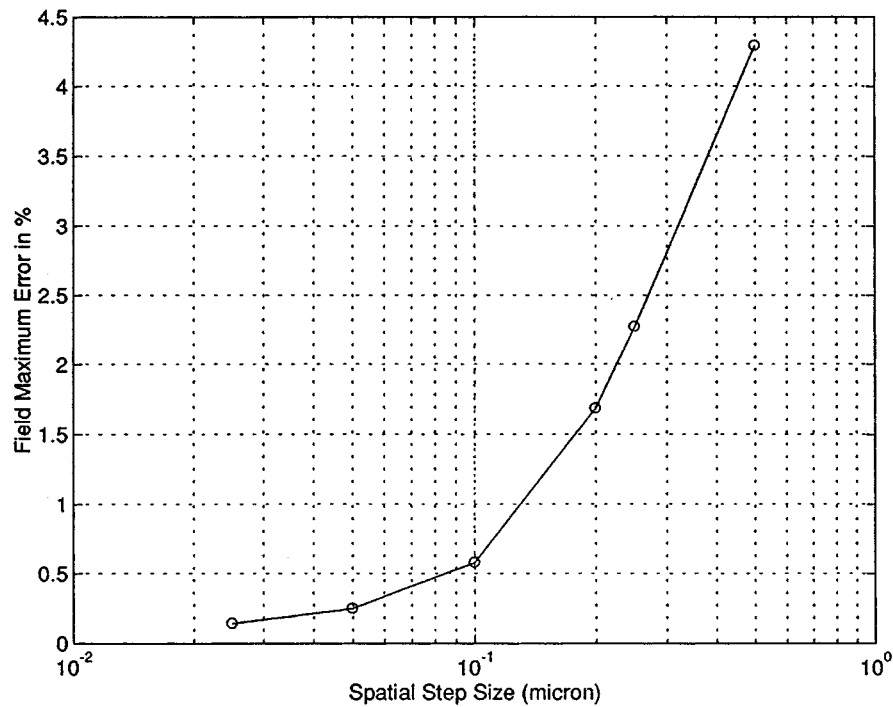


Fig. 7. The percentage maximum error in the field at a distance of $z = 200 \mu\text{m}$ as a function of the spatial step size Δx using the MEFD-TD with $\sigma_{t0} = 100$ fs, $\Delta\tau = 2.0$ fs, and $\lambda = 1.0 \mu\text{m}$.

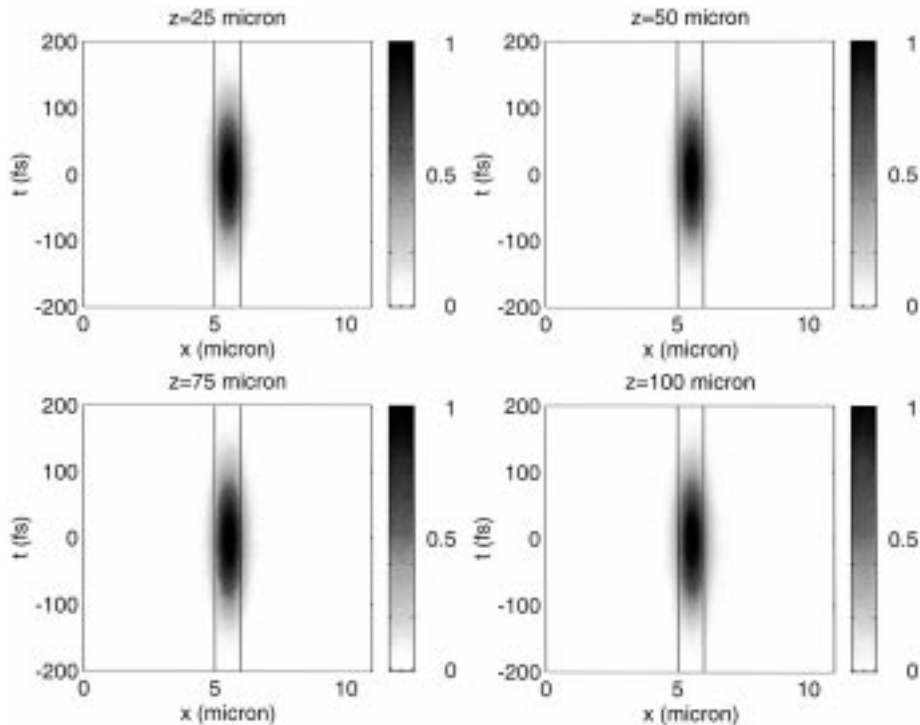


Fig. 8. The evolution of the pulsed first guided mode in the slab dielectric waveguide of Fig. 5 using the MEFD-TD. The reference refractive index was taken to be the effective index of the mode. $d = 1 \mu\text{m}$, $\Delta x = 0.05 \mu\text{m}$, $\Delta\tau = 2.0$ fs, and $\Delta z = 0.008 \mu\text{m}$. A moving time window was used to follow the pulse.

of carrier cycles under the temporal pulse. The figure shows that as the axial angle increases, the relative error increases due to the loss of paraxiality. The figure also shows that increasing the initial pulse width will decrease the error. It is clear that the wider the optical pulse (more carrier cycles), the less the paraxial error.

C. Dielectric Waveguide

In this section, we apply the TD-BPM to simulate the propagation of a temporal pulse in optical dielectric devices. Again, the results are validated with theoretical predictions. We have considered a symmetric dielectric slab waveguide, shown in Fig. 5, with a carrier optical wavelength of $\lambda = 1.0 \mu\text{m}$. The

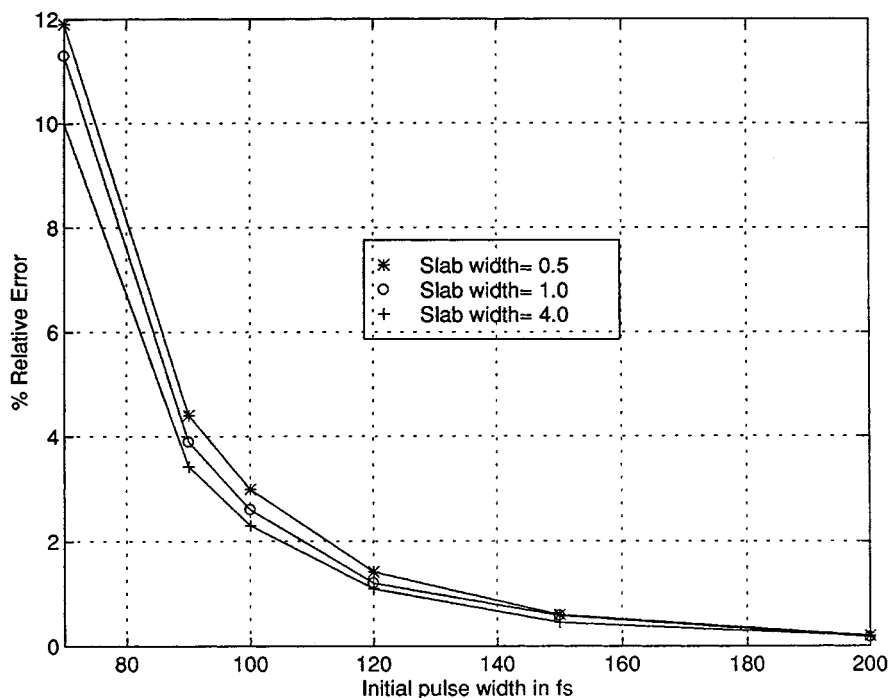


Fig. 9. The percentage relative error of the pulse width, at a distance of half a millimeter ($z = 500 \mu\text{m}$), as a function of the initial pulse width σ_{t_0} for three different slab thicknesses d in μm (of Fig. 5) using MEFD-TD.

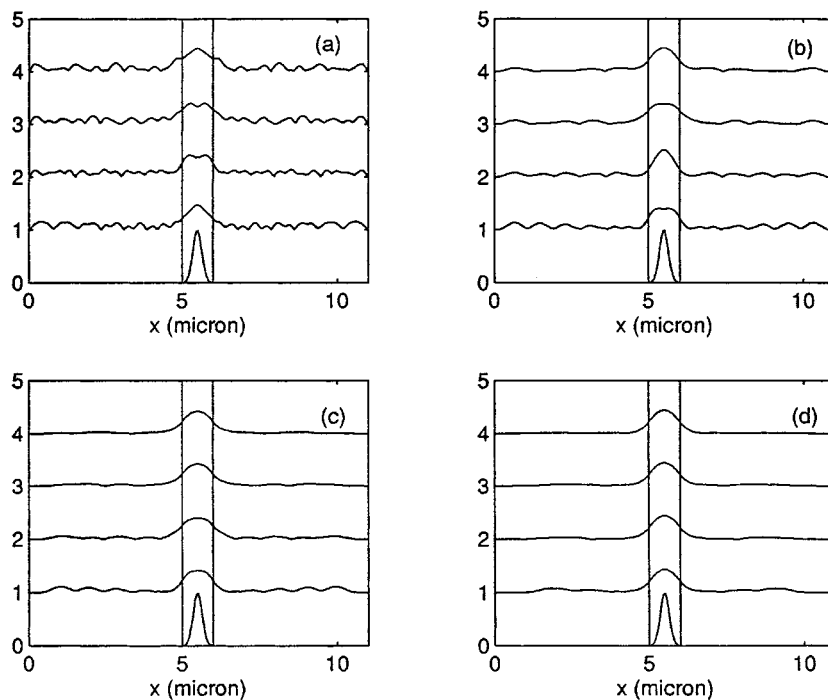


Fig. 10. The propagation of the spatial field using MEFD-TD along the slab dielectric waveguide of Fig. 5 for different spatial PML thickness δ . The fields shown are the input and the propagated fields every $10 \mu\text{m}$ shifted by one from each other for clear presentations. The vertical lines show the position of the slab waveguide. (a) $\delta = 0 \mu\text{m}$ (zero boundary conditions), (b) $\delta = 0.5 \mu\text{m}$, (c) $\delta = 1.0 \mu\text{m}$, and (d) $\delta = 2.0 \mu\text{m}$.

slab waveguide was excited with a pulsed first guided mode shown in Fig. 6 that has a slab width $d = 1 \mu\text{m}$. The temporal input pulse was propagated to a distance of $z = 200 \mu\text{m}$, and then the pulse width is compared with the theoretical value of (22). The dispersion term that appears in this equation was computed numerically from the dispersion relation of a dielectric slab waveguide [33]. Fig. 7 shows the percentage maximum

error in the field, at a distance of $z = 200 \mu\text{m}$, as a function of the spatial step size Δx using the MEFD-TD. The convergence of the MEFD-TD with the reduction of Δx is clearly demonstrated in the figure. On the other hand, Fig. 8 shows the evolution of the pulsed first guide mode along the slab waveguide, of Fig. 5, at different propagational distances using the MEFD-TD. As expected, the figure shows no radiation during

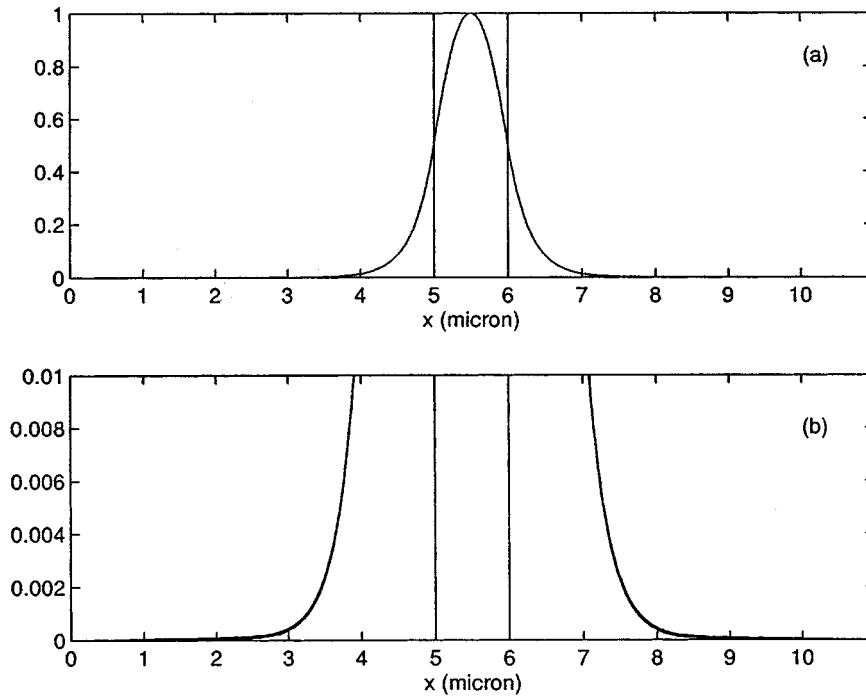


Fig. 11. (a) Comparison between the normalized fields of Fig. 10(c) and Fig. 10(d) at steady state ($z = 200 \mu\text{m}$) and the first guided mode analytical solution. The three fields are indistinguishable. (b) A 1% portion from (a) above shows the three fields closely.

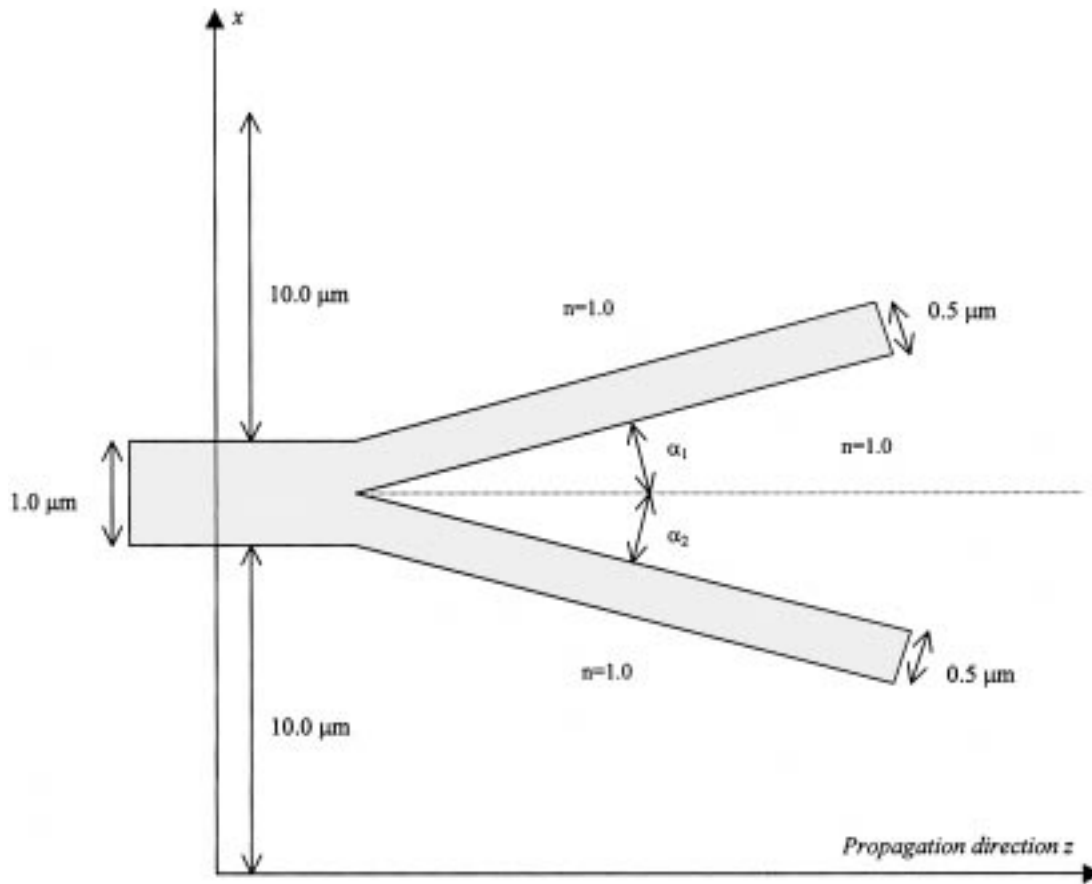


Fig. 12. The two-dimensional Y-junction dielectric waveguide used in the analysis. The main waveguide is that appearing in Fig. 5, and the branched waveguides are single modes with $\lambda = 1.0 \mu\text{m}$ and $n_g = 1.2$.

propagation where the mode in the transverse direction propagates smoothly, and therefore, zero spatial boundary conditions

were used for this simulation. For the purpose of careful analysis, Fig. 9 shows the percentage relative error as a function of

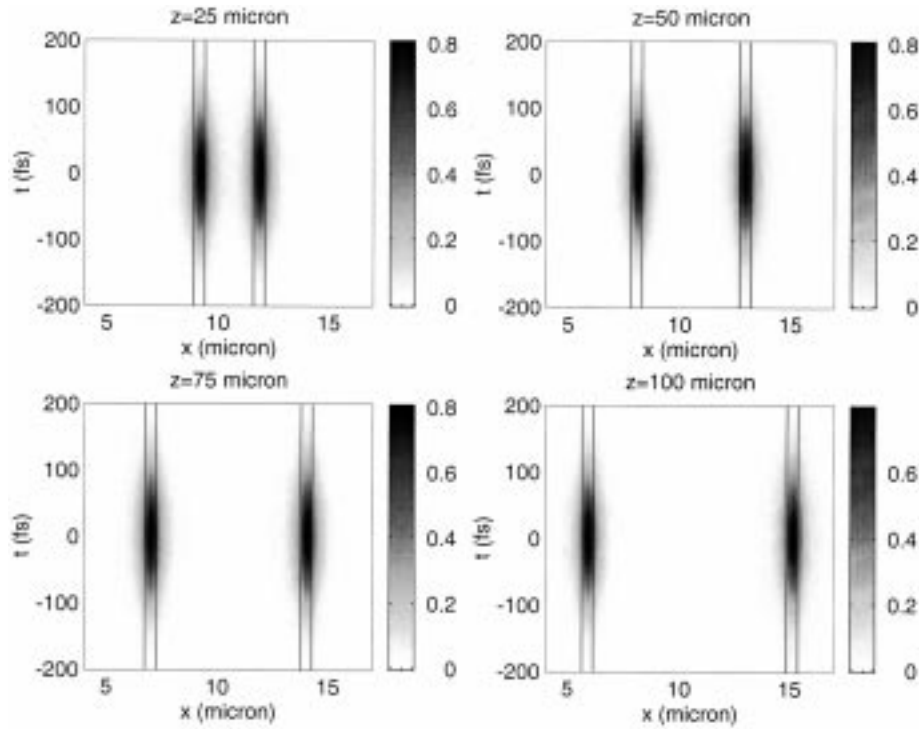


Fig. 13. Field plots for the simulation of the Y-junction of Fig. 12 using MEFD-TD. The input is that of Fig. 5, and the simulation is for a symmetric Y-junction with angles $\alpha_1 = \alpha_2 = 2.5^\circ$. Note that the full window is not shown for clear presentation. The vertical lines on the plots show the analytically predicted positions of the slab waveguides. A moving window was used to follow the pulse. $\Delta x = 0.05 \mu\text{m}$, $\Delta \tau = 2.0 \text{ fs}$, and $\Delta z = 0.008 \mu\text{m}$.

the initial pulse width σ_{t_0} for three different waveguide widths d using the MEFD-TD. The waveguides were excited with their respected pulsed first guided modes. It has to be noticed that changing the width of the waveguide changes the angle of the guided mode. The three slab widths were 0.5 , 1.0 , and $4.0 \mu\text{m}$ corresponding to mode angles of 23.7° , 16.1° , and 5.3° , respectively. It is clear from Fig. 9 that the error associated with the initial pulse width is much more pronounced than that associated with the mode angle. It is to be remembered again that as the pulse width σ_{t_0} increases, the number of cycles under the temporal pulse also increases. The results that appear in Fig. 9 are similar to those appearing in [25], which uses the EFD-TD. We may conclude that the technique can easily handle pulses as short as 100 fs for half a millimeter distance with a relative error of less than 3%; the error decreases by increasing the initial pulse width. The efficiency of the MEFD-TD is quite remarkable with a speed around 0.12 s per propagational step Δz for the simulation of Fig. 8. This is measured on an average 233-MHz Pentium II PC, which means that the whole simulation takes around 25 min to complete.

D. Perfectly Matched Layer

The PML equation given in (13) was used at the transverse spatial dimensions as absorbing boundary conditions. In the PML region, the following graded conductivity distribution is considered [30]:

$$\sigma_x = \sigma_{\max} \left(\frac{\zeta}{\delta} \right)^2 \quad (24)$$

where δ is the thickness of the PML layer at one side and ζ is the distance measured from the interface between the PML layer

and the computational space. The PML medium is terminated by a simple perfectly conducting wall [29]. The maximum conductivity σ_{\max} can be found by requiring the reflection coefficient for the plane wave incident on the interface perpendicular to x (PML region)

$$R(0) = \exp \left[-\frac{2}{3n_p} \sqrt{\frac{\mu_o}{\epsilon_o}} \sigma_{\max} \delta \right] \quad (25)$$

to be smaller than a given value [30]. To examine the performance of the above technique, a pulsed spatial Gaussian optical beam was excited inside the slab dielectric waveguide of Fig. 5 with a slab width of $d = 1.0 \mu\text{m}$ and a carrier wavelength of $\lambda = 1.0 \mu\text{m}$. The initial Gaussian waist was $w_o = 0.2 \mu\text{m}$ and a temporal pulse width of $\sigma_{t_0} = 100 \text{ fs}$. Fig. 10 shows the propagation of the spatial field using the MEFD-TD along the slab waveguide for different spatial PML thickness δ . The fields shown are the transverse spatial fields at the peak of the pulse. In the figure, the fields are the input and the propagated fields every $10 \mu\text{m}$ shifted by one from each other for clear presentations. The maximum conductivity used in all cases was equal $\sigma_{\max} = 0.15 \Omega^{-1} (\mu\text{m})^{-1}$. Comparison among all the results shows the superiority of the PML layer with $\delta = 2 \mu\text{m}$, where the first guided mode of the structure is clearly excited. In addition, Fig. 11 shows a comparison between the normalized transverse spatial fields at steady state ($z = 200 \mu\text{m}$) for the cases of $\delta = 1$ and $\delta = 2 \mu\text{m}$ of the PML and the first guided mode analytical solution. The three fields in Fig. 11(a) are indistinguishable from each other even when 1% of the total field is enlarged [Fig. 11(b)].

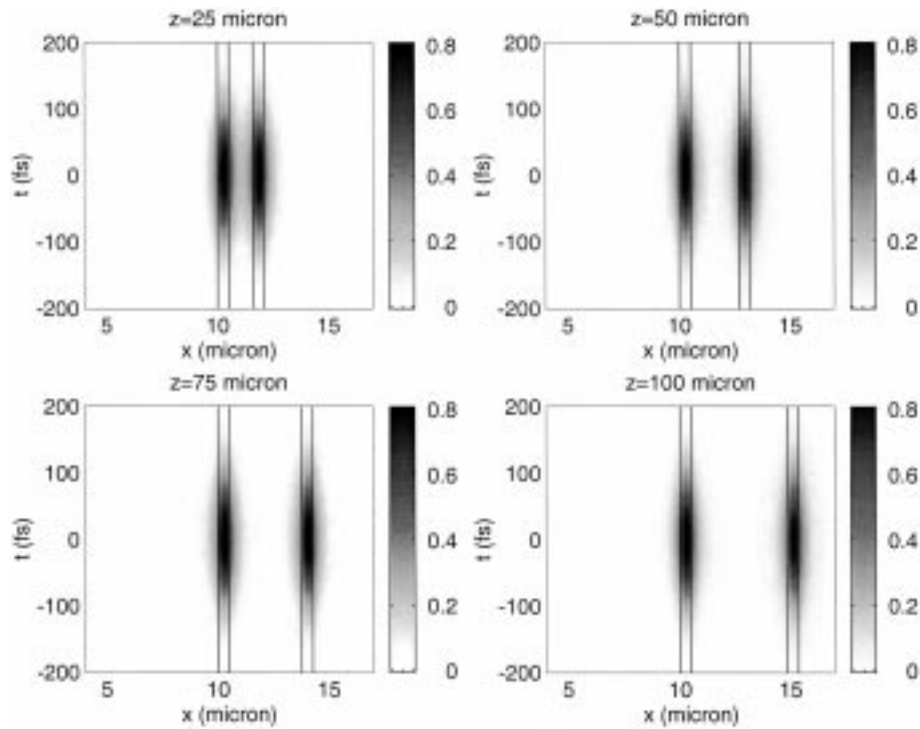


Fig. 14. The simulation is for an asymmetric Y -junction with angles $\alpha_1 = 0.0^\circ$ and $\alpha_2 = 2.5^\circ$. Other parameters are the same as those appearing in Fig. 13.

V. APPLICATION: Y -JUNCTION

In this section, the MEFD-TD has been applied to a two-dimensional dielectric Y -junction waveguide, shown in Fig. 12. The combined waveguide supports two guided modes while each of the branched waveguides is a single mode at the carrier wavelength $\lambda = 1 \mu\text{m}$. The pulsed first guided mode of Fig. 6 was excited at the input of the structure and allowed to propagate inside the Y -junction. Fig. 13 shows the simulation of a symmetric Y -junction when the branched angles are $\alpha_1 = \alpha_2 = 2.5^\circ$. The figure shows field plots for the propagation of the pulsed beam at several distances. Complete symmetrical behavior is observed along the line of symmetry, which is at $x = 10.5 \mu\text{m}$. The lines appearing on the plots are showing the position of the analytically predicted positions of the waveguides. It is to be noticed that in both waveguides, the first guided mode of the new waveguide has been excited where the peak of the mode is appearing in the middle of the guide. In modeling the Y -junction, PML layers were used at the spatial boundary with $\delta = 2 \mu\text{m}$ and $\sigma_{\text{max}} = 0.15 \Omega^{-1} (\mu\text{m})^{-1}$. Fig. 14 shows the simulation of an asymmetric Y -junction using the same parameters of Fig. 13 except that the branched angles are not equal with $\alpha_1 = 0$ and $\alpha_2 = 2.5^\circ$. Clearly, the figure shows an asymmetric propagation for the new modes inside the asymmetric Y -junction.

VI. CONCLUSION

A novel technique to model pulsed optical beams has been introduced and analyzed using linear nondispersive and dispersive examples that have analytical predictions. The derivation, the discretization, and the numerical analysis of the time-domain beam propagation method have been shown in

detail. We have used the explicit finite-difference and the Du Fort–Frankel approaches to discretize the TD-BPM equation, where comparisons between these techniques were also given. The methods were applied to homogenous medium, metallic, and dielectric waveguides; and excellent accuracy results have been observed. It is also shown, similar to their CW counterpart, that both techniques are simple, efficient, and suitable for parallel implementations, especially for 3-D devices. In addition, it was shown that MEFD-TD is more efficient than EFD-TD, where PML layers were used as spatial boundary conditions with MEFD-TD. Then TD-BPM was successfully applied to simulate a dielectric Y -junction structure. It was concluded that the new TD-BPM is particularly well suited to the study of unidirectional propagation of compact temporal pulses over long distances in a guided-wave environment. Future work will focus on the extension of the method to include a wide-angle technique that removes the paraxial limit imposed on the method. In addition, the technique will be examined in the presence of material dispersion, nonlinear parametric optical interactions of $\chi^{(2)}$ and $\chi^{(3)}$, where the time-domain method is essential in order to study the propagation of intense ultrashort pulses.

REFERENCES

- [1] K. S. Yee, "Numerical solution of initial boundary problems involving Maxwell's equations in isotropic media," *IEEE Trans. Antennas Propagat.*, vol. AP-14, pp. 302–307, 1966.
- [2] R. W. Ziolkowski and J. B. Judkins, "Full-wave vector Maxwell equation modeling of the self-focusing of ultrashort optical pulses in a nonlinear Kerr medium exhibiting a finite response time," *J. Opt. Soc. Amer. B*, vol. 10, no. 2, pp. 186–198, Feb. 1993.
- [3] R. W. Ziolkowski, "The incorporation of microscopic material models into the FDTD approach for ultrafast optical pulse simulations," *IEEE Trans. Antennas Propagat.*, vol. 45, pp. 375–391, Mar. 1997.

- [4] R. M. Joseph and A. Taflove, "FDTD Maxwell's equations models for nonlinear electrodynamics and optics," *IEEE Trans. Antennas Propagat.*, vol. 45, pp. 364–374, Mar. 1997.
- [5] A. Taflove, "Review of the formulation and application of the finite-difference time-domain method for numerical modeling of electromagnetic wave interactions with arbitrary structures," *Wave Motion*, vol. 10, pp. 547–582, 1988.
- [6] S. Chu and K. Chaudhuri, "A finite-difference time-domain method for the design and analysis of guided-wave optical structures," *J. Lightwave Technol.*, vol. 7, pp. 2033–2038, 1989.
- [7] W. P. Haung, S. Chu, A. Goss, and K. Chaudhuri, "A scalar finite-difference time-domain approach to guided-wave optics," *IEEE Photon. Technol. Lett.*, vol. 3, pp. 524–526, 1991.
- [8] H. A. Jamid and S. J. Al-Bader, "Finite-difference time-domain approach to nonlinear guided waves," *Electron. Lett.*, vol. 29, pp. 83–84, 1993.
- [9] R. Y. Chan and J. M. Liu, "Time-domain wave propagation in optical structure," *IEEE Photon. Technol. Lett.*, vol. 6, pp. 1001–1003, Aug. 1994.
- [10] P. Liu, Q. Zhao, and F. Choa, "Slow-wave finite-difference beam propagation method," *IEEE Photon. Technol. Lett.*, vol. 7, pp. 890–892, Aug. 1995.
- [11] G. H. Jin, J. Harari, J. P. Viltcot, and D. Decoster, "An improved time-domain beam propagation method for integrated optics components," *IEEE Photon. Technol. Lett.*, vol. 9, pp. 348–350, Mar. 1997.
- [12] J. Zhenle, F. Junmei, and F. Enxin, "An explicit and stable time-domain method for simulation wave propagation in optical structures," *Microw. Opt. Technol. Lett.*, vol. 14, no. 4, pp. 249–252, March 1997.
- [13] F. Ma, "Slowly varying envelope simulation of optical waves in time domain with transparent and absorbing boundary conditions," *J. Lightwave Technol.*, vol. 15, pp. 1974–1985, Oct. 1997.
- [14] L. Gomelsky and J. M. Liu, "Extension of beam propagation method to time dependent optical waveforms," *IEEE Photon. Technol. Lett.*, vol. 6, pp. 546–548, Apr. 1994.
- [15] M. D. Feit and J. A. Fleck, "Light propagation in graded-index optical fibers," *Appl. Opt.*, vol. 17, pp. 3990–3998, 1978.
- [16] D. Yevick, "A guide to electric field propagation techniques for guided-wave optics," *Opt. Quantum Electron.*, vol. 26, pp. 185–197, 1994.
- [17] H. J. W. M. Hoekstra, "On beam propagation methods for modeling in integrated optics," *Opt. Quantum Electron.*, vol. 29, pp. 157–171, 1997.
- [18] Y. Chung and N. Dagli, "Explicit finite difference beam propagation method: Application to semiconductor rib waveguide Y-junction analysis," *Electron. Lett.*, vol. 26, pp. 711–713, 1990.
- [19] —, "Analysis of Z-invariant and Z-variant semiconductor rib waveguides by explicit finite difference beam propagation method with nonuniform mesh configuration," *IEEE J. Quantum Electron.*, vol. 27, pp. 2296–2305, 1991.
- [20] H. M. Masoudi and J. M. Arnold, "Parallel beam propagation methods," *IEEE Photon. Technol. Lett.*, vol. 6, pp. 848–850, 1994.
- [21] —, "Parallel three-dimensional finite-difference beam propagation methods," *Int. J. Numer. Mod.*, vol. 8, pp. 95–107, 1995.
- [22] —, "Parallel beam propagation method for the analysis of second harmonic generation," *IEEE Photon. Technol. Lett.*, vol. 7, pp. 400–402, Apr. 1995.
- [23] —, "Modeling second-order nonlinear effects in optical waveguides using a parallel-processing beam propagation method," *IEEE J. Quantum Electron.*, vol. 31, pp. 2107–2113, Dec. 1995.
- [24] H. M. Masoudi, "Parallel numerical methods for analyzing optical devices with the BPM," Ph.D. dissertation, Faculty of Engineering, Univ. of Glasgow, 1995.
- [25] H. M. Masoudi, M. A. AlSunaidi, and J. M. Arnold, "Time-domain finite-difference beam propagation method," *IEEE Photon. Technol. Lett.*, vol. 11, pp. 1274–1276, Oct. 1999.
- [26] E. C. Du Fort and S. P. Frankel, "Stability conditions in the numerical treatment of parabolic differential equations," *M.T.A.C.*, vol. 7, pp. 135–153, 1953.
- [27] F. Xiang and G. L. Yip, "An explicit and stable finite-difference 2-D vector beam propagation method," *IEEE Photon. Technol. Lett.*, vol. 6, pp. 1248–1250, 1994.
- [28] H. M. Masoudi and J. M. Arnold, "Spurious modes in the Du Fort–Frankel finite-difference beam propagation method," *IEEE Photon. Technol. Lett.*, vol. 9, pp. 1382–1384, Oct. 1997.
- [29] C. M. Rappaport, "Perfectly matched absorbing boundary conditions based on anisotropic mapping of space," *IEEE Microwave Guided Wave Lett.*, vol. 5, pp. 90–92, Mar. 1995.
- [30] W. P. Huang, C. L. Xu, W. Lui, and K. Yokoyama, "The perfectly matched layer (PML) boundary condition for the beam propagation method," *IEEE Photon. Technol. Lett.*, vol. 8, pp. 649–651, May 1996.
- [31] R. W. Ziolkowski and J. B. Judkins, "Propagation characteristics of ultrawide-bandwidth pulsed gaussian beams," *J. Opt. Soc. Amer. A*, vol. 9, no. 11, pp. 2021–2030, Nov. 1992.
- [32] S. Ramo, J. Whinnery, and T. V. Duzer, *Fields and Waves in Communication Electronics*. New York: Wiley, 1984.
- [33] D. L. Lee, *Electromagnetic Principles of Integrated Optics*. New York: Wiley, 1986.
- [34] K. L. Shalager, J. G. Maloney, S. L. Ray, and A. F. Peterson, "Relative accuracy of several finite-difference time-domain methods in two and three dimensions," *IEEE Trans. Antennas Propagat.*, vol. 41, pp. 1732–1737, Dec. 1993.

Husain M. Masoudi received the B.S. and M.S. degrees from the Electrical Engineering Department of King Fahd University of Petroleum and Minerals (KFUPM) at Dhahran, Saudi Arabia, in 1986 and 1989, respectively. He also received the Ph.D. degree in opto-electronics from the Electronics and Electrical Engineering Department in the University of Glasgow, U.K., in 1995.

From 1989 to 1991, he taught undergraduate courses of electromagnetic theory, electronics, and circuit analysis in the same department as a Lecturer. In 1995, he was appointed as an Assistant Professor in the Department of Electrical Engineering at KFUPM. In 1998, he was also assigned to be a Manager of Laser Research Section, Center for Applied Physical Sciences, Research Institute at KFUPM. In addition, he is also the Coordinator of Optical Device Simulation Group (ODSG) <http://www.kfupm.edu.sa/odsg/> Electrical Engineering Department of KFUPM, Saudi Arabia. His current research interest is modeling linear and non-linear optical devices; this includes both continuous wave (CW) interactions and pulsed optical beams.

Muhammad A. Al-Sunaidi received the B.S. and M.S. degrees in electrical engineering from King Fahd University of Petroleum and Minerals (KFUPM), Dhahran, Saudi Arabia, in 1984 and 1987, respectively, and the Ph.D. degree in electrical engineering from Arizona State University, Tempe, AZ, in 1995.

Between 1987 and 1991, he was a Lecturer in the Electrical Engineering Department, KFUPM, where he taught courses in electronics, digital design and electromagnetics. In 1991, he joined the Ph.D. program at Arizona State University, where he was a Research Assistant in the Solid State Research Center and the Telecommunication Research Center between 1991 and 1993 and between 1993 and 1995, respectively. Since May 1995, he has been with KFUPM, where he is now an Assistant Professor in the Department of Electrical Engineering. His research activities include modeling and simulation of high-frequency active devices, optically controlled active devices, computational electromagnetics, and nonlinear integrated optics.

Dr. Alsunaidi received a number of international research fellowships including the British Council Research Award at the University of Glasgow in 1998 and the Matsumae International Foundation Award at Tokai University, Japan, in 2000.

John M. Arnold, photograph and biography not available at the time of publication.